Journal of Molecular Structure 1209 (2020) 127940

Contents lists available at ScienceDirect

Journal of Molecular Structure

journal homepage: http://www.elsevier.com/locate/molstruc

Synthesis, spectroscopic characterization, crystal structure, DFT, molecular docking and *in vitro* antibacterial potential of novel quinoline derivatives

Younos Bouzian [a], Khalid Karrouchi [b, *], Yusuf Sert [c], Chin-Hung Lai [d, e, **], Lhassane Hani [f], Noureddine Hamou Ahabchane [a], Ahmed Talbaoui [g], Joel T. Mague [h], El Mokhtar Essassi [a]

[a] Laboratory of Heterocyclic Organic Chemistry, Department of Chemistry, Faculty of Sciences, Mohamed V University, BP1014, Rabat, 10100, Morocco
[b] Laboratory of Medicinal Chemistry, Faculty of Medicine and Pharmacy, University Mohammed V, Rabat, Morocco
[c] Sorgun Vocational School, Science and Art Faculty-Department of Physics, Yozgat Bozok University, Yozgat, Turkey
[d] Department of Medical Applied Chemistry, Chung Shan Medical University, Taichung, 40241, Taiwan
[e] Department of Medical Education, Chung Shan Medical University Hospital, 402, Taichung, Taiwan
[f] Moroccan Foundation for Advanced Science, Innovation and Research (Mascir), Department of Nanotechnology. Rabat Design Center, Rue Mohamed Al Jazouli, Madinat Al Irfane Rabat, 10 100, Morocco
[g] Laboratoire de Biologie des Pathologies Humaines, Faculté des Sciences, Université Mohammed V, Rabat, Morocco
[h] Department of Chemistry, Tulane University, New Orleans, LA, 70118, USA

ARTICLE INFO

Article history:
Received 14 January 2020
Received in revised form
18 February 2020
Accepted 19 February 2020
Available online 22 February 2020

Keywords:
Synthesis
Quinoline
X-ray analysis
DFT
Hirshfeld surface analysis
Antibacterial activity
Molecular docking

ABSTRACT

Two novel quinolone derivatives were prepared and characterized using different spectroscopic techniques and single crystal X-ray diffraction. The DFT-B3LYP study was also performed to investigate differences in the electric properties. The *in vitro* antibacterial activity of two compounds was investigated against *Escherichia coli* ATCC4157, *Pseudomonas aeruginosa* ATCC 27853, *Staphylococcus aureus* ATCC 25923 and *Streptococcus faecalis* ATCC 29212 bacterial strains and the results obtained showed the remarkable activity of **2** and **3** towards *S. aureus* and *E. coli*. with MIC values of 6.25 μg/mL compared to standard. Molecular docking was performed to position compounds **2** and **3** into the *S. aureus* 1JIJ active site to rationalize the probable mode of action, binding affinity, and orientation of the molecules at the active site of receptor.

1. Introduction

Heterocyclic compounds have paved the way for exceptional achievements in the fight against many life-threatening diseases [1]. It is therefore no surprise that the development of new methodologies to synthesize biologically active heterocyclic compounds is a very important goal in organic chemistry [2]. Quinoline derivatives represent an important class of bioactive heterocyclic compounds in the field of pharmaceuticals [3]. The quinoline ring system possesses various pharmacological properties such as antibacterial [4], antileishmanial [5], antitubecular [6], anti-inflammatory [7], antimalarial [8], anti-HCV [9], antiviral [10], anticancer [11], anti-alzheimer [12], analgesic [13], cardiovascular [14], antibiotic [15], tyrosine kinase (PDGF-RTK) inhibition [16] and antihypertensive activities [17]. The synthetic antibacterial agents that include levofloxacin, ciprofloxacin and norfloxacin belong to the quinolone class of compounds, sharing quinoline as the basic ring skeleton (Fig. 1). In view of the biological importance of quinoline derivatives, the determinations of the structural, geometric and electronic properties of these derivatives are essential to know the influence of different groups on structures in order to discover the relationship of these groups with their pharmacological properties.

Currently, computational approaches constitute a solid

* Corresponding author.
** Corresponding author. Department of Medical Applied Chemistry, Chung Shan Medical University, Taichung, 40241, Taiwan.
E-mail addresses: Khalid.karrouchi@um5s.net.ma (K. Karrouchi), chlai125@csmu.edu.tw (C.-H. Lai).

https://doi.org/10.1016/j.molstruc.2020.127940
0022-2860/

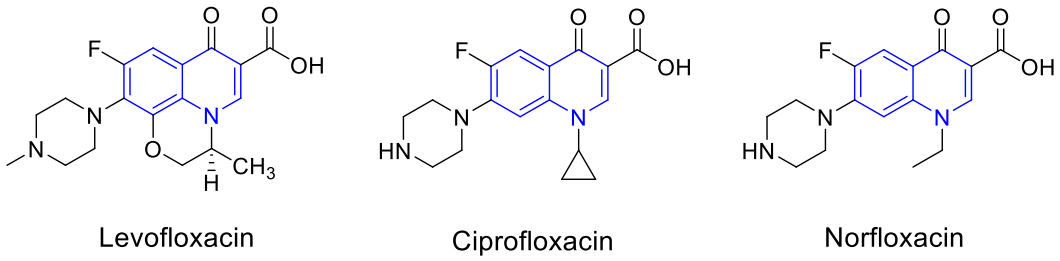

Fig. 1. Structures of the standard quinoline antibiotics.

complement to experimental data for the interpretation of results. In particular, functional density theory (DFT) has become a very important and frequently used tool for researching experimental data and in studies of biological systems. A varied range of calculations using DFT helps to develop a close relationship between theoretical and experimental data by giving clues related to molecular geometry, electrical and spectroscopic properties. In the modern era, these techniques have become very reliable in predicting the properties of molecules with great precision [18–23]. In a continuation of our research work on the development of new quinoline derivatives likely to have potential pharmacological activities [23–25], two new quinoline derivatives namely, dodecyl 2-(dodecyloxy)quinoline-4-carboxylate (**2**) and dodecyl 1-dodecyl-2-oxo-1,2-dihydroquinoline-4-carboxylate (**3**) (Fig. 2), have been synthesized and characterized by spectroscopic techniques (FT-IR, ^{1}H NMR, ^{13}C NMR and ESI-MS). The molecular structure of **2** has been determined by single crystal X-ray diffraction. The puckering parameters of the non-planar rings of the title molecule have also been obtained. The antibacterial activity of the new compounds against a variety of bacterial strains has also been investigated. The results obtained from theoretical calculations using the DFT-B3LYP method are compared with the experimental ones. Molecular docking was performed using the crystal structure of *S. aureus* tyrosyl-tRNA synthetase (PDB: 1JIJ) in complex with **2** and **3** to explore the binding modes of these compounds at the active site.

2. Experimental

2.1. General methods

Reactions were checked with TLC using aluminum sheets with silica gel 60 F254 from Merck. Melting points were measured using a Buchi B-545 digital capillary melting point apparatus and are uncorrected. The FT-IR spectrum was recorded with PerkinElmer VERTEX 70 FT-IR spectrometer over the range 400–4000 cm^{-1}.^{1}H and ^{13}C NMR spectra were recorded in DMSO-d_6 solutions on a Bruker spectrometer (300 MHz). The chemical shifts are expressed in parts per million (ppm) from tetramethylsilane (TMS) as an internal reference. Mass spectra were obtained using an API 3200 LC/MS/MS system equipped with an ESI source. Chemical reagents were purchased from Fluka, Sigma and Aldrich chemicals.

*General procedure for the synthesis of **2** and **3***: A mixture of 2-oxo-1,2-dihydroquinoline-4-carboxylic acid (0.8 g, 4.23 mmol), K_2CO_3 (1.28 g, 9.41 mmol), *n*-dodecyl bromide (2.25 mL, 9.41 mmol) and tetra *n*-butylammonium bromide as a catalyst in DMF (50 mL) was stirred at room temperature for 48 h. After removal of the salts by filtration, the solvent was evaporated under reduced pressure and the residue obtained was dissolved in dichloromethane. The organic phase was dried over Na_2SO_4 and concentrated under vacuum. The crude product obtained was purified by chromatography on a column of silica gel (eluent: hexane) to afford two new compounds **2** and **3** respectively (Scheme 1).

Dodecyl 2-(dodecyloxy)quinoline-4-carboxylate (2)

Colorless crystals, Yield = 44%, m.p = 35 °C; IR (ν (cm^{-1})): 2958 (C–H), 2917–2847 (CH_2, CH_3) 1714 (C=O), 1603 (C=C), 1462 (C=N); Yield (%) = 44; ^{1}H NMR (300 MHz, $CDCl_3$) δ 8.63 (dd, J = 8.4, 1.0 Hz, 1H, CH_{ar}), 7.91 (dd, J = 8.4, 0.7 Hz, 1H, CH_{ar}), 7.68 (m, 1H, CH_{ar}), 7.52–7.43 (m, 2H, CH_{ar}, CH_{pyr}), 4.52 (t, J = 6.7 Hz, 2H, CH_2–O), 4.44 (t, J = 6.7 Hz, 2H, CH_2–N), 1.95–1.22 (m, 40H, CH_2), 0.92 (t, J = 6.6 Hz, 6H, CH_3). ^{13}C NMR (75 MHz, $CDCl_3$) δ 166.04(C=O), 161.60 (C=O), 147.65, 138.24, 121.95 (Cq), 129.76, 127.72, 125.56, 115.39(CH_{ar}) 124.99(=CH), 66.43, 65.95(CH_2–O), 31.94, 29.70,

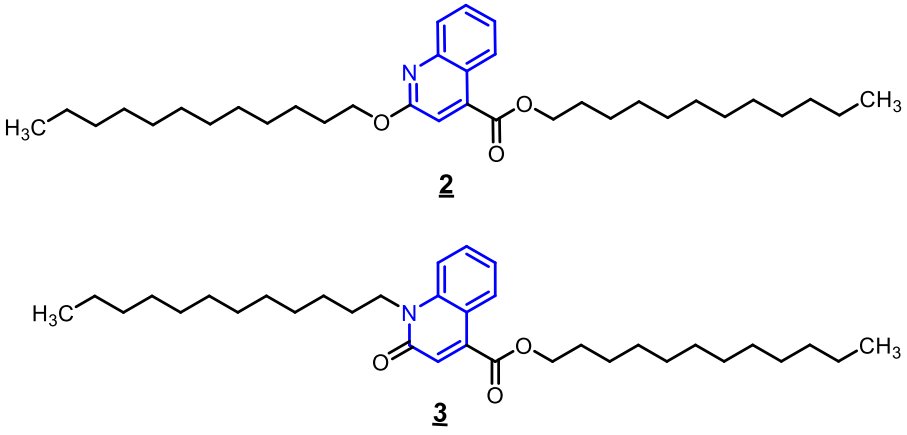

Fig. 2. The structures of **2** and **3**.

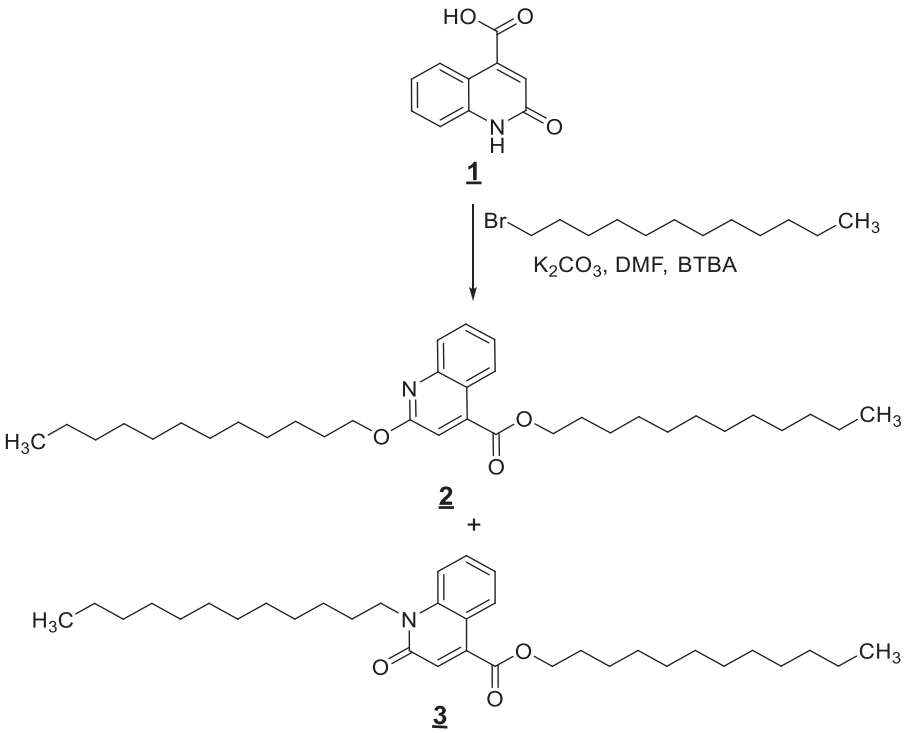

Scheme 1. Synthetic route to **2** and **3.**

29.67, 29.65, 29.60, 29.53, 29.45, 29.38, 29.28, 28.98, 28.65, 26.14, 26.06, 22.72 (CH_2), 14.15 (CH_3); ESI-MS: $m/z = 526.4$ $[M+H]^+$.

Dodecyl 1-dodecyl-2-oxo-1,2-dihydroquinoline-4-carboxylate (3)

White solid, Yield = 45%, m.p = 61 °C; IR (ν (cm^{-1})): 3471 (NH), 1652 (C═O), 1602 (C═N); ^{1}H NMR (300 MHz, $CDCl_3$) δ 8.38 (dd, $J = 8.2$, 1.2 Hz, 1H, CH_{ar}), 7.67–7.59 (m, 1H, CH_{ar}), 7.43 (d, $J = 8.5$ Hz, 1H, CH_{ar}), 7.33–7.28 (m, 2H,CH_{ar}, CH_{pyr}), 4.41 (t, $J = 6.6$ Hz, 2H, CH_2–O), 4.37–4.29 (t, $J = 6.6$ Hz, 2H, CH_2–N), 1.87–1.24 (m, 40H, CH_2), 0.91 (t, $J = 6.6$ Hz, 6H, CH_3). ^{13}C NMR (75 MHz, $CDCl_3$) δ 165.58 (C═O), 161.17(C═O), 139.59, 138.88, 122.44 (Cq) 131.02, 127.35, 124.16, 114.55 (CH_{ar}), 117.81 (=CH), 66.17 (CH_2–O), 42.73 (CH_2–N), 31.93, 29.65, 29.64, 29.59, 29.52, 29.39, 29.36, 29.26, 28.59, 27.45, 27.04, 26.00, 22.71(CH_2), 14.14(CH_3). ESI-MS: $m/z = 526.5$ $[M+H]^+$, 548.4 $[M+Na]^+$.

2.2. Computational details

The structures of **2** and **3** in the gas phase were optimized by density functional theory. The DFT calculations were performed by the hybrid B3LYP method, which is based on the idea of Becke and consider a mixture of the exact (HF) and DFT exchange using the B3 functional, together with the LYP correlation functional in conjunction with the basis set def2-SVP [26–29]. After obtaining the converged geometry, the harmonic vibrational frequencies were calculated at the same theoretical level to confirm the number of imaginary frequencies is zero for the stationary point. All the DFT calculations of **2** and **3** were done with the Gaussian 16 program [30].

Both the definition of a molecule in a condensed phase and the recognition of distinct entities in molecular liquids and crystals are fundamental concepts in chemistry. Based on Hirshfeld's partitioning scheme, Spackman et al. in 1997 proposed a method to divide the electron distribution in a crystalline phase into molecular fragments [31–33]. Their proposed method partitioned the crystal into regions where the electron distribution of a sum of spherical atoms for the molecule dominates over the corresponding sum of the crystal. Because it derived from Hirshfeld's stockholder partitioning, the molecular surface is named the Hirshfeld surface. In this study, the Hirshfeld surface analysis of the title compound was performed using the Crystal Explorer program [34]. Finally, molecular docking studies between **2** and **3** and tyrosyl-tRNA synthetase (PDB: 1JIJ) were carried out employing the AutoDockVina free software program [35].

2.3. X-ray analysis

A single colorless crystal of dimension 0.093 × 0.137 × 0.260 mm^3 of **2** was selected and X-ray intensity data were collected at 150 K on a Bruker D8 VENTURE PHOTON 100 CMOS diffractometer equipped with an X-ray generator operating at 50 kV and 1 mA, using Cu-Kα radiation of wavelength 1.54178 Å. The hemisphere of data was processed using *SAINT* [36]. The 3D structure was solved by direct methods and refined by full-matrix least squares method on F^2 using the *SHELXL* program [37,38]. All the non-hydrogen atoms were revealed in the first difference Fourier map and were refined with isotropic displacement parameters. At the end of the refinement, the final difference Fourier map showed no peaks of chemical significance and the final residual was 0.0641. The molecular and packing diagrams were generated using DIAMOND [39].

2.4. Antibacterial activity

Compounds were evaluated for their *in vitro* antibacterial activity against *E. coli*, *P. aeruginosa*, *S. aureus* and *S. faecalis* which were procured from the Department of Biology, Faculty of Science, Rabat, Morocco. The agar dilution method was performed using Mueller–Hinton agar (Hi-media) plates (37 °C, 24 h) [40].

Suspensions of each microorganism were prepared to contain approximately 10^6 colonies forming units (CFU) ml and applied to plates with serially diluted compounds to be tested and incubated at 37 °C overnight. The minimum inhibitory concentration (MIC) was considered as the lowest concentration that completely inhibited the growth on agar plates, disregarding a single colony or faint haze caused by the inoculum.

3. Results and discussion

3.1. Description of crystal structure

The asymmetric unit of **2** contains two independent molecules differing in the conformations of the dodecyl chain of the ester. The two dodecyl chains are in “fully extended” conformations giving the molecules a “V" shape (Fig. 3). Neither quinoline moiety is quite planar. For the molecule containing N1, the dihedral angle between the constituent planes is 2.23 (3)° while for the molecule containing N2 the dihedral angle is 1.2 (3)°. In the crystal, stacks extending along the *a*-axis direction are formed by slipped π-stacking interactions between quinoline moieties (Fig. 4). These are connected into thick layers along the c-axis direction by C—H···O hydrogen bonds (Table 2). Unlike related molecules, there is minimal intercalation of the alkyl chains (Fig. 5).

The details of the crystal data and structure refinement are given in Table 1.

3.2. DFT calculations

Due to the differences in the hybridization of the nitrogen and oxygen atoms, these should influence the geometry of the pyridine ring. Therefore, the DFT-B3LYP method was used to investigate differences in their gas-phase geometry. Their B3LYP-optimized geometries are shown in Fig. 6. As expected, the B3LYP-optimized geometry of the pyridine ring in **2** showed some differences with respect to that in **3**.

3.3. Hirshfeld surface analysis

The standard resolution molecular Hirshfeld surface (d_{norm}) of **3** is shown in Fig. 7. The surface is shown as transparent so the molecular moiety can be visualized in a similar orientation for all the structures around which they were calculated. The 3D d_{norm} surface can be used to identify very close intermolecular interactions. The value of d_{norm} is negative (positive) when intermolecular contacts

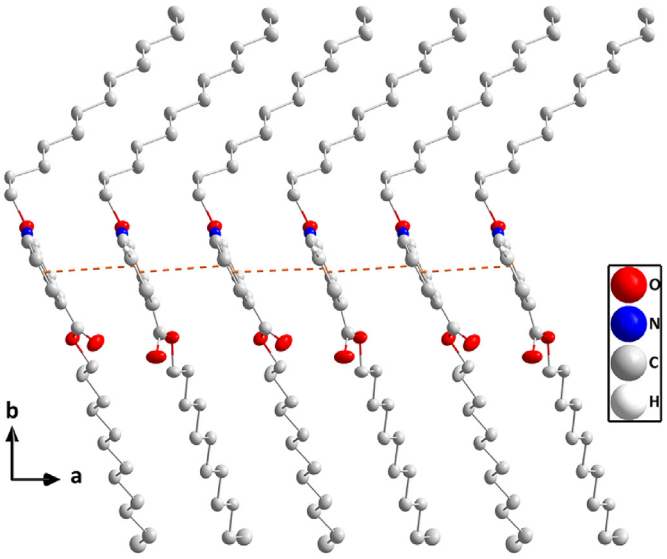

Fig. 4. A portion of one stack formed by π-stacking interactions (dashed lines) viewed along the *c*-axis direction.

are shorter (longer) than the van der Waals radii. The d_{norm} value is mapped onto the Hirshfeld surface by red, white or blue colors. The red regions represent closer contacts with a negative d_{norm} value while the blue regions represent longer contacts with a positive d_{norm} value. Moreover, the white regions represent contacts equal to the van der Waals separation and have a d_{norm} value of zero. As depicted in Fig. 7, the important interactions in the title compound may be the H···O hydrogen bond. In order to understand the importance of H···O hydrogen bonds in **3**, we further performed the investigation about the 2D fingerprint plots of the title compound (Fig. 8).

The 2D fingerprint plots highlight particular atom pair contacts and enable the separation of contributions from different interaction types that overlap in the full fingerprint. Using the standard 0.6–2.6 view with the d_e and d_i distance scales displayed on the graph axes and including the reciprocal contacts, we found the most important interaction involving hydrogen in **2** was the H···H contact. Although **2** contains nitrogen, the contribution of the H···N hydrogen bond was calculated to be negligibly small. The contributions of the H···O, H···N, and H···H contacts are 5.2%, 0.8%, and 86.2%, respectively.

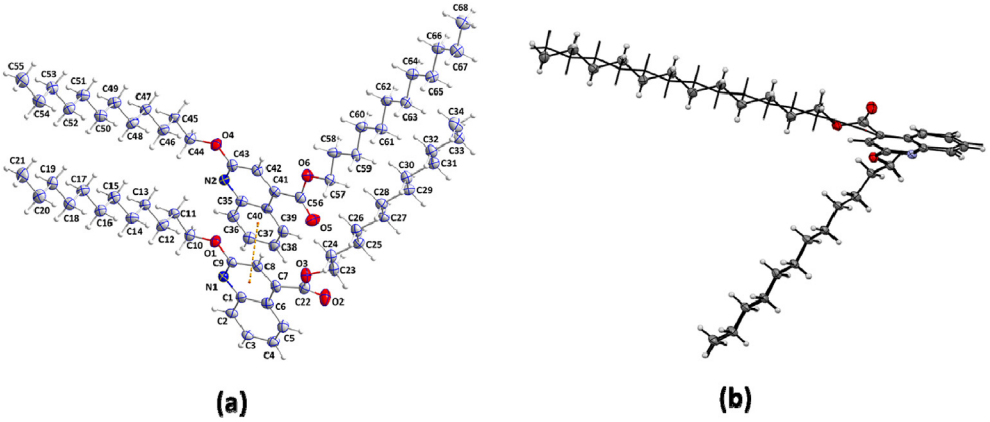

Fig. 3. The asymmetric unit with labeling scheme and 50% probability ellipsoids. The π-stacking interaction is shown by a dashed line (a); Superimposition of the two molecules in the asymmetric unit showing the opposite orientations of the ester substituent (b).

Table 1
Crystallographic and refinement data for **2.**

CCDC Deposition Number	CCDC 1965624
Chemical formula	$C_{34}H_{55}NO_3$
M_r	525.79
Crystal system, space group	Monoclinic, $P2_1$
Temperature (K)	150
a, *b*, *c* (Å)	8.3477 (2), 45.7449 (11), 9.0616 (2)
β (°)	116.168 (1)
V (Å^3)	3105.64 (13)
Z	4
Radiation type	Cu *Kα*
μ (mm^{-1})	0.54
Crystal size (mm)	0.26 × 0.14 × 0.09
Data collection	
Diffractometer	Bruker D8 VENTURE PHOTON 100 CMOS
Absorption correction	Multi-scan *SADABS* [41]
T_{min}, T_{max}	0.87, 0.95
No. of measured, independent and observed [$I > 2\sigma(I)$] reflections	24,746, 9702, 7223
R_{int}	0.065
$(\sin\theta/\lambda)_{max}$ (Å^{-1})	0.610
Refinement	
R [$F^2 > 2\sigma(F^2)$], wR (F^2), S	0.064, 0.150, 1.06
No. of reflections	9702
No. of parameters	689
No. of restraints	1
H-atom treatment	H-atom parameters constrained
$\Delta\rho_{max}$, $\Delta\rho_{min}$ (e Å^{-3})	0.24, −0.21

Table 2
Hydrogen-bond geometry (Å, °).

D—H···*A*	*D*—H	*H*···*A*	*D*···*A*	*D*—H···*A*
C3—H3···O1^{i}	0.95	2.59	3.535 (6)	172

Symmetry code: (i) *x*, *y*, *z*+1

3.4. Antibacterial activity

The antibacterial activities of **1**, **2** and **3** were tested against *E. coli*, *P. aeruginosa*, *S. aureus* and *Streptococcus faecalis* microorganisms. The results obtained were compared with Chloramphenicol and Ampicilline as standards, with different concentrations. A comparative study of minimum inhibitory concentration (MIC) values of **1**, **2** and **3** indicates that **2** and **3** have better activity (Table 3 and Fig. 9). As shown in Table 3, it is obvious that **2** and **3** have higher antibacterial activities against *S. aureus* and *E. coli*. Compound **2** has strong activity against *S. aureus* with MIC value of 6.25 μg/mL, even better than the effect of chloramphenicol and ampicilline. Compound **3** has strong activity against *E. coli*, with MIC value of 6.25 μg/mL, which is comparable to chloramphenicol. Compound **3** showed outstanding activity against *S. aureus* and *S. faecalis*, with MIC value of 12.5 μg/mL. Compounds **2** and **3** have medium activity against *P. aeruginosa*, with MIC value of 50 and 25 μg/mL, respectively.

3.5. Molecular docking

Molecular docking is both an effective and reliable theoretical method considering the results it produces in drug design. Here, the binding interactions of ligands with the target protein or enzyme are generally through intermolecular bonds. In other words, this method is crucial in drug design and is frequently the preferred way for estimating the bioactive conformation of the ligand in the protein binding region [42,43]. In the antibacterial activity experiments (section 3.3), **2** and **3** showed substantial activity against *E. coli*, *P. aeruginosa*, *S. aureus* and *S. faecalis* microorganisms. The starting three-dimensional structure of *S. aureus* tyrosyl-tRNA synthetase (PDB: 1JIJ) was taken from the Protein Data Bank (PDB) [44]. Before molecular docking calculations, it is necessary to remove all natural ligands attached to the receptor molecule to clear the active site for more efficient calculations. The active sites of PDB: 1JIJ protein were determined to be ASN199, GLN196, ASP195, GLY193, ASP177, GLN174, TYR170, ASP80, LEU70,

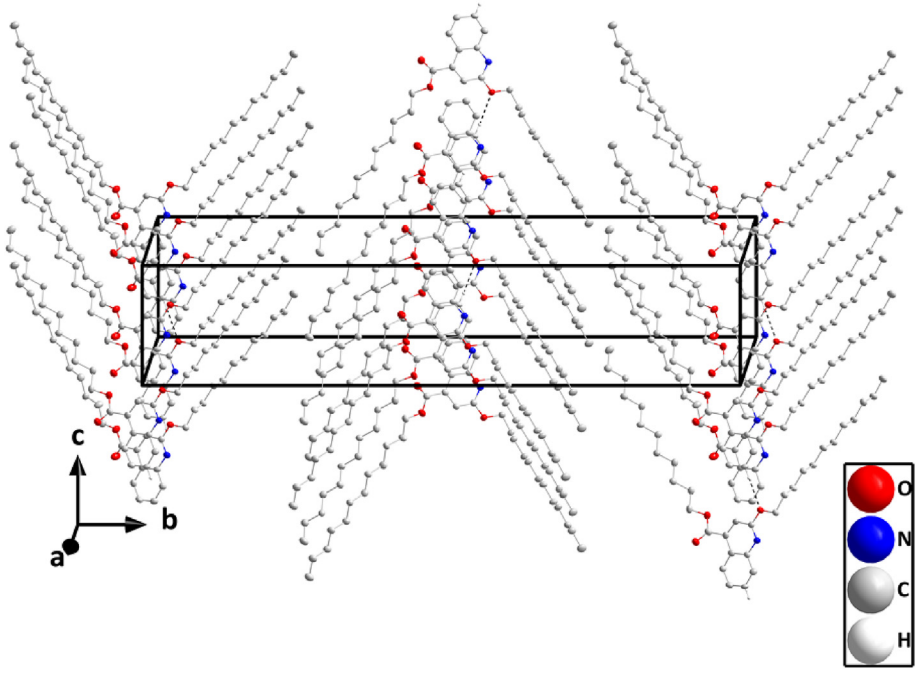

Fig. 5. Packing showing the intercalation of alkyl chains from neighboring stacks. C—H···O hydrogen bonds are depicted by black dashed lines.

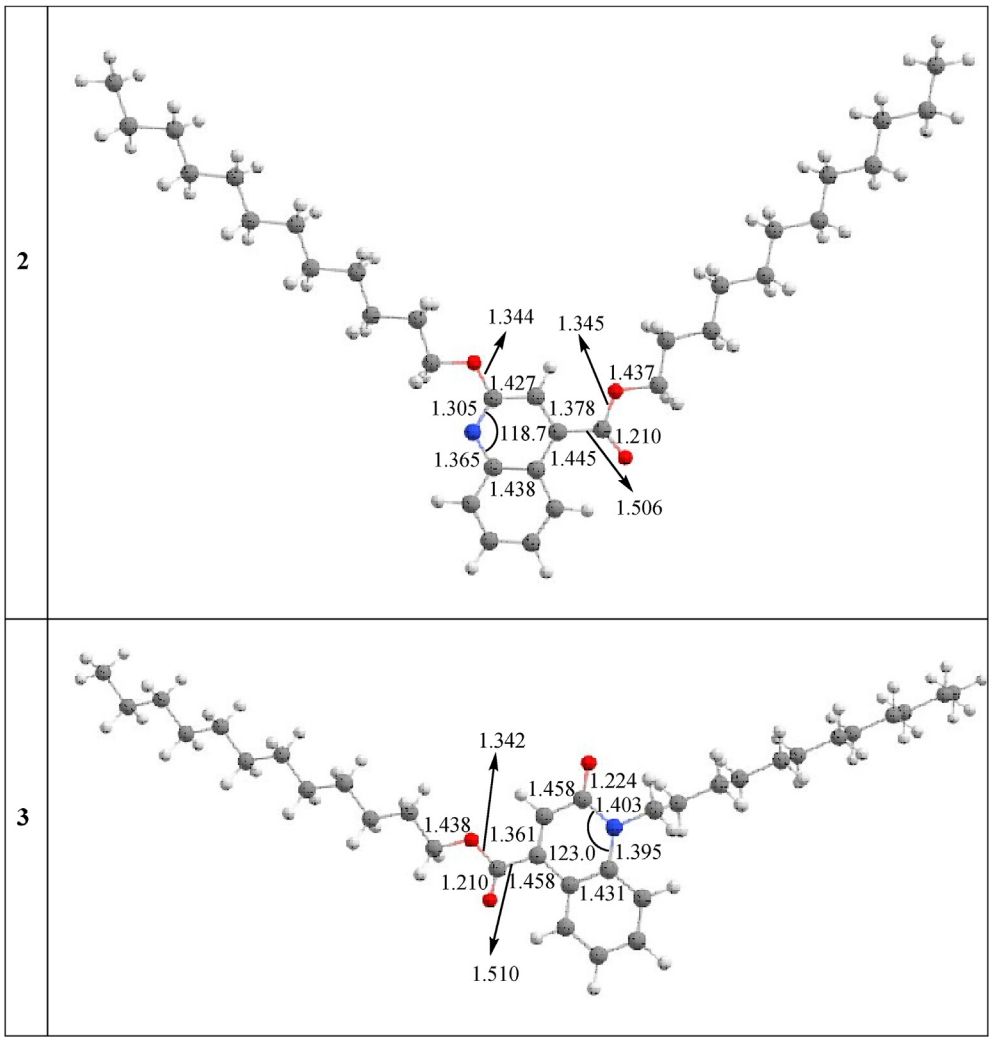

Fig. 6. The B3LYP-optimized geometries of **2** and **3** (bond lengths in Å, and bond angle in °).

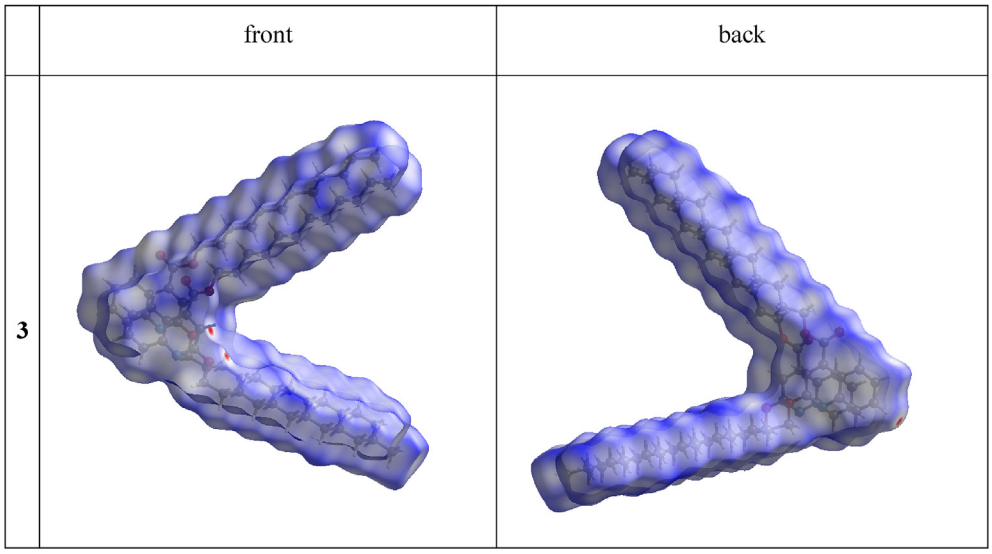

Fig. 7. The dnorm Hirshfeld surface of the title compound (red: negative, white: zero, blue: positive; scale: −0.1054 to 1.3928 a.u.).

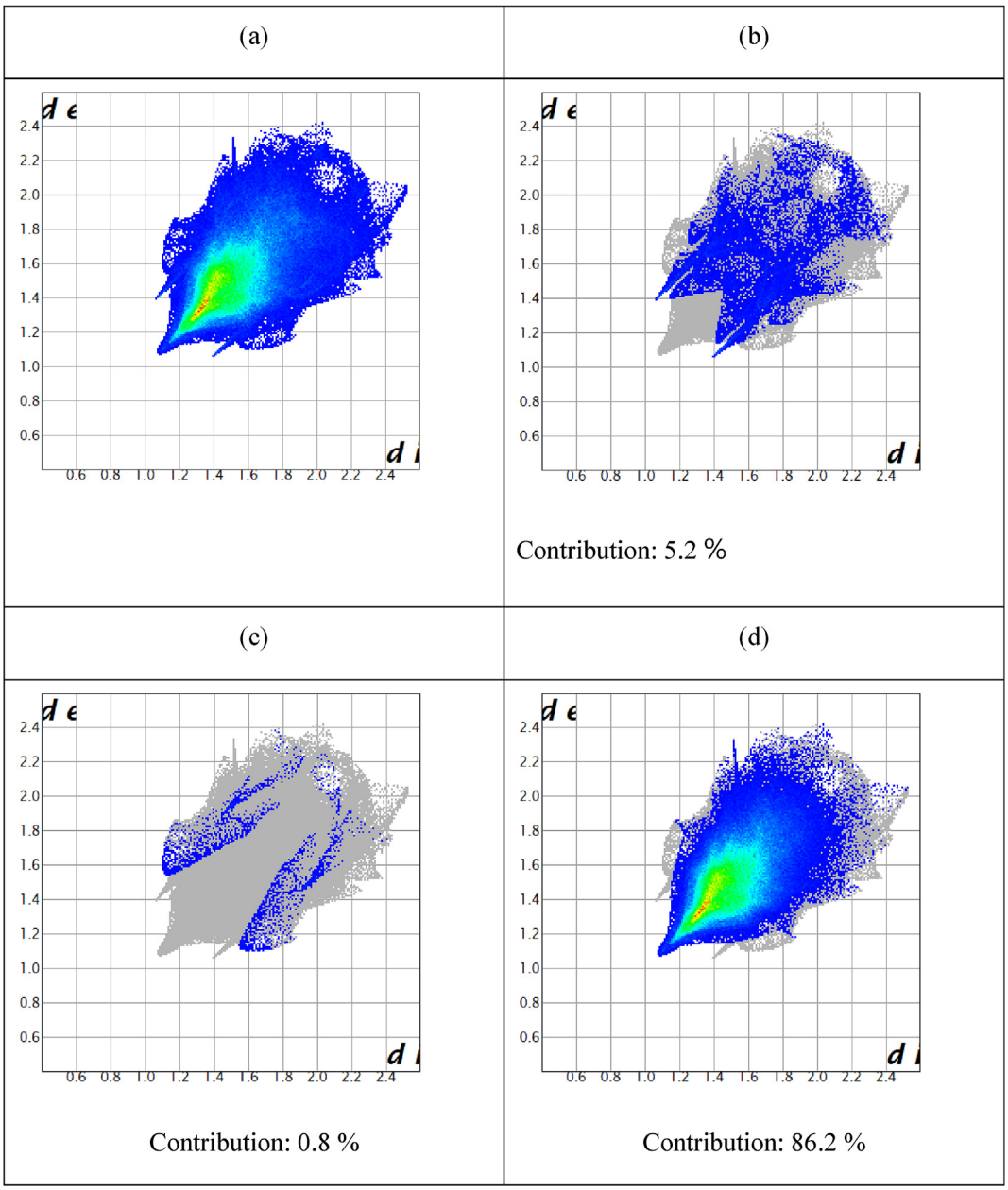

Fig. 8. The 2D fingerprint plot of the title compound (a) full, (b) resolved by the H···N contacts, (c) resolved by the H···O contacts, (d) resolved by the H···H contacts.

Table 3
MIC of synthesized compounds against growth of bacteria (μg.mL-1).

Compounds	*E. coli*	*P. aeruginosa*	*S. aureus*	*S. faecalis*
1	50	50	50	50
2	12.5	50	6.25	25
3	6.25	25	12.5	12.5
Chloramphenicol	6.25	6.25	12.5	12.5
Ampicilline	12.5	25	12.5	6.25

HIS50, GLY49, ASP40, ALA39, GLY38 and TYR36. Then grid box sizes were determined as 46 × 58 × 48 $Å^3$ and x, y, z centers: −11.685, 16.111, and 84.367, and the 1JIJ protein were recorded in PDBQT format. In the next step, **2** and **3** were optimized with B3LYP/GEN, the optimized structure was converted into PDB format and the rotatable angles for the ligate structures were determined and recorded as PDBQT. All preparations for **2** and **3** ligands and receptor protein 1JIJ were carried out with the Discover Studio Visualizer 4.0 (DSV 4.0) software [45]. Molecular docking calculations were performed by using the AutoDock Vina program [35] and ten different conformations were determined for the ligands which are within the protein receptor. The **2**+1JIJ and **3**+1JIJ molecular docking interactions were evaluated and tabulated in Table S1 (Supporting Information). According to the affinity binding energies, the best binding was observed in mode 1 with an energy of −6.9 kcal/mol) and three hydrogen bonding interactions. The interaction types between protein and **3** are indicated in Fig. 10 where 2 of the 3 conventional hydrogen bonds were observed in the active region of PDB: 1JIJ (Fig. 10a) between the TYR170 residue and N15 and between the GLY38 residue and O18 at distances of 6.56 and 3.31 Å, respectively. Also, a conventional hydrogen bond was observed in the inactive site of 1JIJ protein between the CYS37

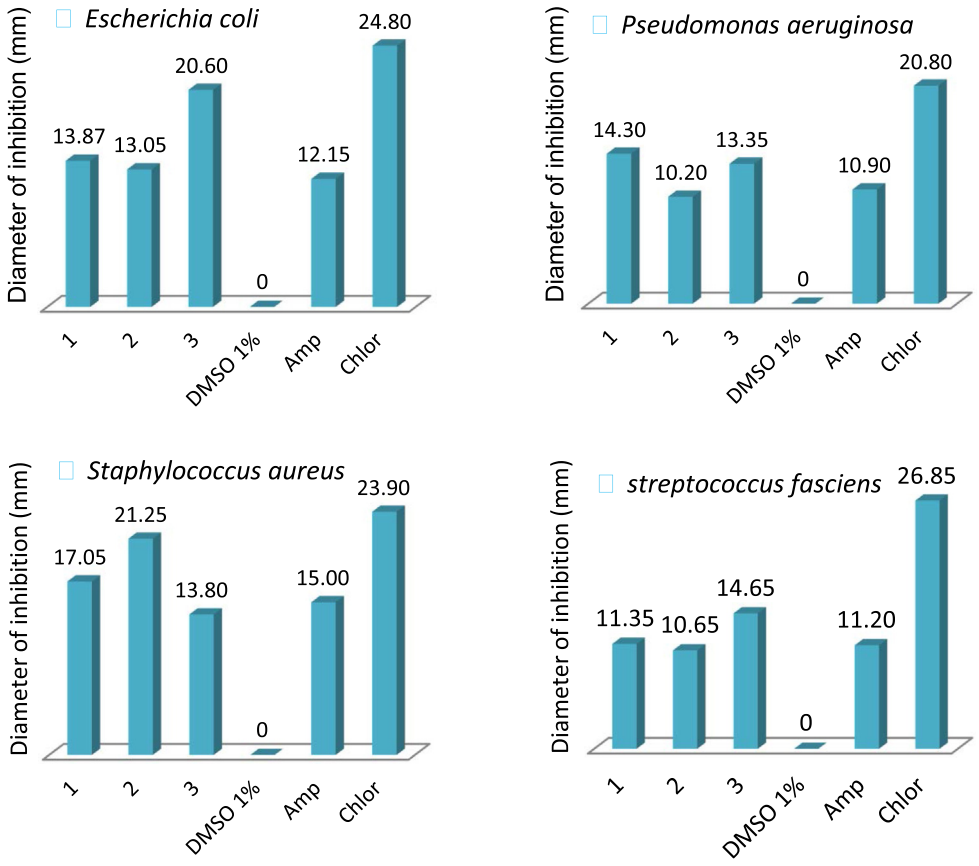

Fig. 9. Diameter of inhibition of synthesized compounds and controls.

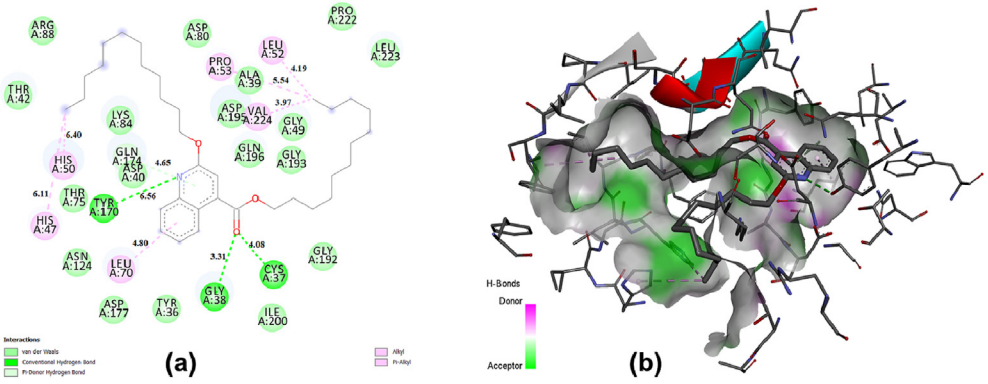

Fig. 10. The molecular docking results of **2** with 1JIJ protein, 2D forms (a) and 3D forms (b).

residue and O18 at a 4.08 Å distance. Additionally in Fig. 10, van der Waals, π-donor hydrogen bond, alkyl and π-alkyl interactions and their bonding distances are shown.

The interaction parameters between PDB: 1JIJ receptor and **2** were obtained and are given in Table S1 (Supporting Information). According to the affinity binding energies, the best binding was observed in mode 1 with energy of −6.7 kcal/mol and two conventional hydrogen bonds. The interaction types between protein and **3** are presented in Fig. 11. It is important to note that none of these interactions occur with the active site of the protein. The conventional hydrogen bonds between LYS4 and O56 and GLN196 and O55 have 3.17 Å and 3.24 Å distances, respectively. Apart from these interactions, there are van der Waals, carbon-hydrogen bond, π-anion, π-π stacked, alkyl and π-alkyl interactions and their distances were shown in Fig. 11. Additionally, the docking conditions between **2**+1JIJ and **3**+1JIJ can be easily seen in Fig. 12.

As a result, the theoretical *in silico* based molecular docking scores support that **2** and **3** are potent antibacterial inhibitors. The theoretical results agree with experimental antibacterial activities.

4. Conclusion

In this work, two novel quinoline derivatives namely: Dodecyl 1-dodecyl-2-oxo-1,2-dihydroquinoline-4-carboxylate (**2**) and

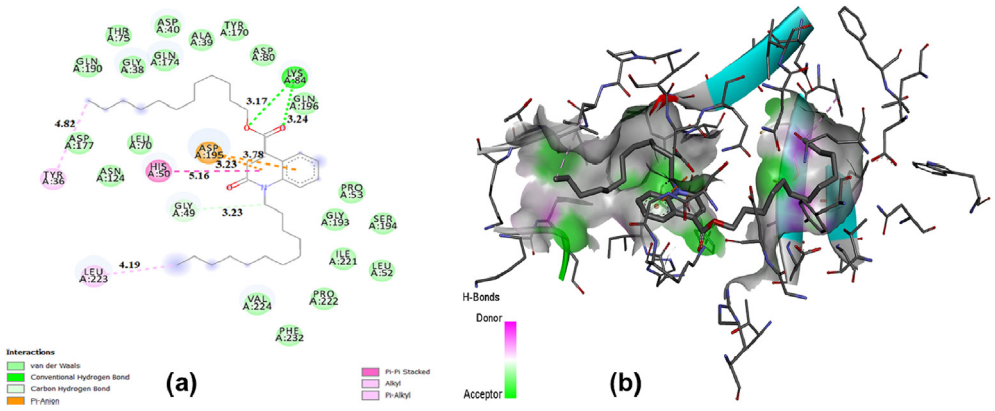

Fig. 11. The molecular docking results of **3** with 1JIJ protein, 2D forms (a) and 3D forms (b).

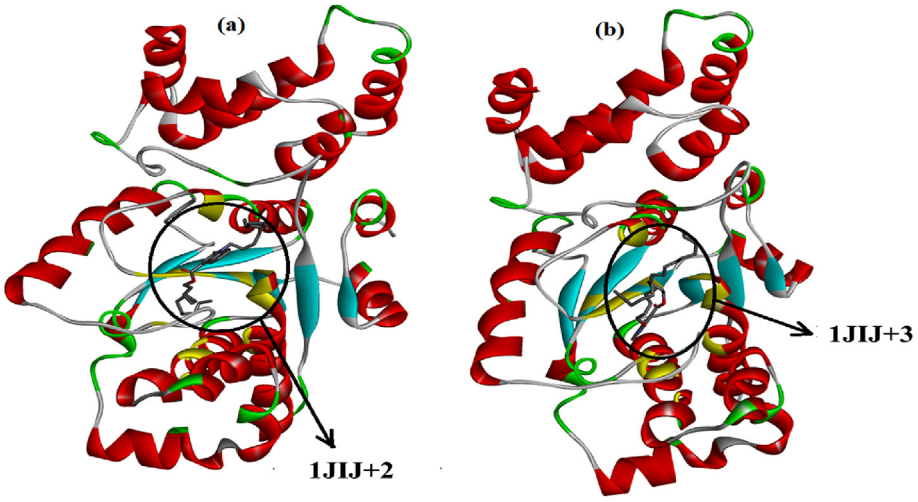

Fig. 12. The three-dimensional structure of 1JIJ protein with the title molecules **2** and **3**.

dodecyl 2-tridecylquinoline-4-carboxylate (**3**) have been synthesized and characterized by means of ^{1}H and ^{13}C NMR, FT-IR spectroscopy, ESI-MS spectrometry and by single crystal X-ray diffraction studies. The DFT-B3LYP and Hirshfeld surface analysis were also performed to investigate their differences in the electric properties to confirm the existence of intermolecular interactions. In addition, *in vitro* antibacterial activity against *E. coli*, *P. aeruginosa*, *S. aureus* and *S. fasciens* showed that **2** and **3** exhibit a high antibacterial activity against *S. aureus* and *E. coli* with MIC values of 6.25 μg/mL. Molecular docking studies revealed that various interactions tightly anchored the title compounds to the active site, which could well explain their excellent antibacterial activities.

CRediT author statement

Younos Bouzian and Khalid Karrouchi: Realization of the experiments, treatment of the results and bibliographical research. Involved in compounds synthesis and characterization. Peparation of protocols, participation in the interpretation, writing and manuscript review. Yusuf Sert: Performed the molecular docking study and description. Chin-Hung Lai: Performed the DFT calculations. Joel T. Mague: Determined the X-ray crystal structure. Lhassane Hani: Carried out the NMR analysis and interpretation. Ahmed Talbaoui: Carried out the antibacterial activity. Noureddine Hamou Ahabchane: Cooperated in the preparation of the manuscript, interpretation of the results. El Mokhtar Essassi: Research director, coordination of work, concept development, Supervision of experiments as well as Formal analysis and processing of results.

Declaration of competing interests

The authors declare that they have no known competing financial interests or personal relationships that could have appeared to influence the work reported in this paper.

Acknowledgment

This work is supported by UM5R, we would like to acknowledge the UATRS-CNRST and Analysis and Characterization Platform ACP-FSR. The support of NSF-MRI Grant #1228232 for the purchase of the diffractometer and Tulane University for support of the Tulane Crystallography Laboratory are gratefully acknowledged. We also thank the National Center for High-performance Computing (Taiwan) for providing computing time.

Appendix A. Supplementary data

Supplementary data to this article can be found online at https://doi.org/10.1016/j.molstruc.2020.127940.

References

[1] B. Alcaide, P. Almendros, C. Aragoncillo, Highly reactive 4-membered ring nitrogen-containing heterocycles: synthesis and properties, Curr. Opin. Drug Disc. 13 (2010) 685–697.

[2] S.B. Jones, B. Simmons, A. Mastracchio, D.W. MacMillan, Collective synthesis of natural products by means of organocascade catalysis, Nature 475 (2011) 183–188.

[3] X.M. Chu, C. Wang, W. Liu, L.L. Liang, K.K. Gong, C.Y. Zhao, K.L. Sun, Quinoline and quinolone dimers and their biological activities: an overview, Eur. J. Med. Chem. 161 (2019) 101–117.

[4] S.S. Panda, S. Liaqat, A.S. Girgis, A. Samir, C.D. Hall, A.R. Katritzky, Novel antibacterial active quinolone–fluoroquinolone conjugates and 2D-QSAR studies, Bioorg. Med. Chem. Lett 25 (18) (2015) 3816–3821.

[5] P. Palit, P. Paira, A. Hazra, S. Banerjee, A.D. Gupta, S.G. Dastidar, N.B. Mondal, Phase transfer catalyzed synthesis of bis-quinolines: antileishmanial activity in experimental visceral leishmaniasis and in vitro antibacterial evaluation, Eur. J. Med. Chem. 44 (2) (2009) 845–853.

[6] Z. Xu, C. Gao, Q.C. Ren, X.F. Song, L.S. Feng, Z.S. Lv, Recent advances of pyrazole-containing derivatives as anti-tubercular agents, Eur. J. Med. Chem. 139 (2017) 429–440.

[7] R. de Meneses Santos, P.R. Barros, J.H. Bortoluzzi, M.R. Meneghetti, Y.K.C. da Silva, A.E. da Silva, M.S. Alexandre-Moreira, Synthesis and evaluation of the anti-nociceptive and anti-inflammatory activity of 4-aminoquinoline derivatives, Bioorg. Med. Chem. 23 (15) (2015) 4390–4396.

[8] L. Van Heerden, T.T. Cloete, J.W. Breytenbach, C. de Kock, P.J. Smith, J.C. Breytenbach, D.D. N'Da, Synthesis and in vitro antimalarial activity of a series of bisquinoline and bispyrrolo [1, 2a] quinoxaline compounds, Eur. J. Med. Chem. 55 (2012) 335–345.

[9] R. Cannalire, M.L. Barreca, G. Manfroni, V. Cecchetti, A journey around the medicinal chemistry of hepatitis C virus inhibitors targeting NS4B: from target to preclinical drug candidates, J. Med. Chem. 59 (1) (2015) 16–41.

[10] K.C. Sekgota, S. Majumder, M. Isaacs, D. Mnkandhla, H.C. Hoppe, S.D. Khanye, F.H. Kriel, J. Coates, P.T. Kaye, Application of the Morita-Baylis-Hillman reaction in the synthesis of 3-[(N-cycloalkylbenzamido) methyl]-2-quinolones as potential HIV-1 integrase inhibitors, Bioorg. Chem. 75 (2017) 310–316.

[11] Q. Tang, Y. Duan, H. Xiong, T. Chen, Z. Xiao, L. Wang, Y. Xiao, S. Huang, Y. Xiong, W. Zhu, P. Gong, P. Zheng, Synthesis and antiproliferative activity of 6, 7-disubstituted-4-phenoxyquinoline derivatives bearing the 1, 8-naphthyridin-2-one moiety, Eur. J. Med. Chem. 158 (2018) 201–213.

[12] M.L. Bolognesi, A. Cavalli, L. Valgimigli, M. Bartolini, M. Rosini, V. Andrisano, M. Racanatini, C. Melchiorre, Multi-target-directed drug design strategy: from a dual binding site acetylcholinesterase inhibitor to a trifunctional compound against Alzheimer's disease, J. Med. Chem. 50 (26) (2007) 6446–6449.

[13] A. Mai, D. Rotili, D. Tarantino, A. Nebbioso, S. Castellano, G. Sbardella, L. Altucci, Identification of 4-hydroxyquinolines inhibitors of p300/CBP histone acetyltransferases, Bioorg. Med. Chem. Lett 19 (4) (2009) 1132–1135.

[14] T.A. Rano, E. Sieber-McMaster, P.D. Pelton, M. Yang, K.T. Demarest, G.H. Kuo, Design and synthesis of potent inhibitors of cholesteryl ester transfer protein (CETP) exploiting a 1, 2, 3, 4-tetrahydroquinoline platform, Bioorg. Med. Chem. Lett 19 (9) (2009) 2456–2460.

[15] A. Mahamoud, J. Chevalier, A. Davin-Regli, J. Barbe, Quinoline derivatives as promising inhibitors of antibiotic efflux pump in multidrug resistant Enterobacter aerogenes isolates, Curr. Drug Targets 7 (7) (2006) 843–847.

[16] M.P. Maguire, K.R. Sheets, K. McVety, A.P. Spada, A. Zilberstein, A new series of PDGF receptor tyrosine kinase inhibitors: 3-substituted quinoline derivatives, J. Med. Chem. 37 (14) (1994) 2129–2137.

[17] N. Muruganantham, R. Sivakumar, N. Anbalagan, V. Gunasekaran, J. T. Leonard Synthesis, Anticonvulsant and antihypertensive activities of 8-substituted quinoline derivatives, Biol. Pharm. Bull. 27 (10) (2004) 1683–1687.

[18] I. Chakib, Y. El Bakri, C.H. Lai, L. Benbacer, A. Zerzouf, E.M. Essassi, J. T. Mague Synthesis, Anticancer evaluation in vitro, DFT, Hirshfeld surface analysis of some new 4-(1, 3-benzothiazol-2-yl)-3-methyl-1-phenyl-4, 5-dihydro-1H-pyrazol-5-one derivatives, J. Mol. Struct. 1198 (2019) 126910.

[19] B. Sureshkumar, Y.S. Mary, C.Y. Panicker, S. Suma, S. Armaković, S.J. Armaković, C.V. Alsenoy, B. Narayana, Quinoline derivatives as possible lead compounds for anti-malarial drugs: spectroscopic, DFT and MD study, Arabian J. Chem. 13 (2020) 632–648.

[20] K. Karrouchi, E. Yousfi, N. Sebbar, Y. Ramli, J. Taoufik, Y. Ouzidan, A. M'hammed, Y.N. Mabkhot, H.A. Ghabbour, S. Radi, New pyrazole-hydrazone derivatives: X-ray analysis, molecular structure investigation via density functional theory (DFT) and their high in-situ catecholase activity, Int. J. Mol. Sci. 18 (11) (2017) 2215.

[21] R.R. Pillai, K. Karrouchi, S. Fettach, S. Armaković, S.J. Armaković, Y. Brik, J. Taoufik, S. Radi, M.E.A. Faouzi, M. H. Ansar Synthesis, Spectroscopic characterization, reactive properties by DFT calculations, molecular dynamics simulations and biological evaluation of Schiff bases tethered 1, 2, 4-triazole and pyrazole rings, J. Mol. Struct. 1177 (2019) 47–54.

[22] Y. Xue, Y. Liu, L. An, L. Zhang, Y. Yuan, J. Mou, Y. Zheng, Electronic structures and spectra of quinoline chalcones: DFT and TDDFT-PCM investigation, Comput. Theor. Chem. 965 (2011) 146–153.

[23] Y.F. Baba, Y. Sert, Y.K. Rodi, S. Hayani, J.T. Mague, D. Prim, J. Marrot, F. Ouazzani Chahdi, N.K. Sebbar, E.M. Essassi, Synthesis, crystal structure, spectroscopic characterization, Hirshfeld surface analysis, molecular docking studies and DFT calculations, and antioxidant activity of 2-oxo-1, 2-dihydroquinoline-4-carboxylate derivatives, J. Mol. Struct. 1188 (2019) 255–268.

[24] Y. Bouzian, M.S.H. Faizi, J.T. Mague, B.E. Otmani, N. Dege, K. Karrouchi, E.M. Essassi, Crystal structure and DFT study of benzyl 1-benzyl-2-oxo-1, 2-dihydroquinoline-4-carboxylate, Acta Crystallogr. 75 (7) (2019) 980–983.

[25] Y. Bouzian, K. Karrouchi, E.H. Anouar, R. Bouhfid, S. Arshad, E.M. Essassi, Crystal structure, DFT study and Hirshfeld surface analysis of ethyl 6-chloro-2-ethoxyquinoline-4-carboxylate, Acta Crystallogr. 75 (6) (2019) 912–916.

[26] A.D. Becke, Density-functional thermochemistry. III. The role of exact exchange, J. Chem. Phys. 98 (1993) 5648–5652.

[27] C. Lee, W. Yang, R.G. Parr, Development of the Colle-Salvetti correlation-energy formula into a functional of the electron density, Phys. Rev. B 37 (1988) 785–789.

[28] B. Miehlich, A. Savin, H. Stoll, H. Preuss, Results obtained with the correlation energy density functionals of becke and Lee, Yang and Parr, Chem. Phys. Lett. 157 (1989) 200–206.

[29] F. Weigend, R. Ahlrichs, Balanced basis sets of split valence, triple zeta valence and quadruple zeta valence quality for H to Rn: design and assessment of accuracy, Phys. Chem. Chem. Phys. 7 (2005) 3297–3305.

[30] M.J. Frisch, G.W. Trucks, H.B. Schlegel, G.E. Scuseria, M.A. Robb, J.R. Cheeseman, G. Scalmani, V. Barone, G.A. Petersson, H. Nakatsuji, X. Li, M. Caricato, A.V. Marenich, J. Bloino, B.G. Janesko, R. Gomperts, B. Mennucci, H.P. Hratchian, J.V. Ortiz, A.F. Izmaylov, J.L. Sonnenberg, D. Williams-Young, F. Ding, F. Lipparini, F. Egidi, J. Goings, B. Peng, A. Petrone, T. Henderson, D. Ranasinghe, V.G. Zakrzewski, J. Gao, N. Rega, G. Zheng, W. Liang, M. Hada, M. Ehara, K. Toyota, R. Fukuda, J. Hasegawa, M. Ishida, T. Nakajima, Y. Honda, O. Kitao, H. Nakai, T. Vreven, K. Throssell, J.A. Montgomery Jr., J.E. Peralta, F. Ogliaro, M.J. Bearpark, J.J. Heyd, E.N. Brothers, K.N. Kudin, V.N. Staroverov, T.A. Keith, R. Kobayashi, J. Normand, K. Raghavachari, A.P. Rendell, J.C. Burant, S.S. Iyengar, J. Tomasi, M. Cossi, J.M. Millam, M. Klene, C. Adamo, R. Cammi, J.W. Ochterski, R.L. Martin, K. Morokuma, O. Farkas, J.B. Foresman, D.J. Fox, Gaussian 16, Revision A.03, Gaussian, Inc., Wallingford CT, 2016.

[31] M.A. Spackman, P.G. Byrom, A novel definition of a molecule in a crystal, Chem. Phys. Lett. 267 (1997) 215–220.

[32] J.J. McKinnon, M.A. Spackman, A.S. Mitchell, Novel tools for visualizing and exploring intermolecular interactions in molecular crystals, Acta Crystallogr. B60 (2004) 627–668.

[33] M.A. Spackman, D. Jayatilaka, Hirshfeld surface analysis, CrystEngComm 11 (2009) 19–32, 2009.

[34] M.J. Turner, J.J. McKinnon, S.K. Wolff, D.J. Grimwood, P.R. Spackman, D. Jayatilaka, M.A. Spackman, CrystalExplorer17, University of Western Australia, 2017.

[35] O. Trott, A.J. Olson, AutoDock Vina, Improving the speed and accuracy of docking with a new scoring function, efficient optimization, and multithreading, J. Comput. Chem. 31 (2) (2010) 455–461.

[36] Bruker, APEX3, SAINT, SADABS & SHELXTL, Bruker AXS, Inc., Madison, WI, 2016.

[37] G.M. Sheldrick, Acta Crystallogr. A71 (2015) 3–8.

[38] G.M. Sheldrick, Acta Crystallogr. C71 (2015) 3–8.

[39] K. Brandenburg, H. Putz, DIAMOND, Crystal Impact GbR, Bonn, Germany, 2012.

[40] A. Talbaoui, N. Jamaly, A.I. Idrissi, M. Bouksaim, S. Gmouh, M. El Moussaouiti, A. Benjouad, Y. Bakri, J. Med. Plants Res. 6 (31) (2012) 4593–4600.

[41] L. Krause, R. Herbst–Irmer, G.M. Sheldrick, D. Stalke, Comparison of silver and molybdenum microfocus X-ray sources for single-crystal structure determination, J. Appl. Crystallogr. 48 (2015) 3–10.

[42] U. Kragh-Hansen, Molecular aspects of ligand binding to serum albumin, Pharm. Rev. 33 (1) (1981) 17–53.

[43] U. Kragh-Hansen, Relations between high-affinity binding sites of markers for binding regions on human serum albumin, Biochem. J. 225 (3) (1985) 629–638.

[44] https://www.rcsb.org/.

[45] https://www.3dsbiovia.com/.